Clays and Clay Minerals, Vol. 43, No. 3, 271–284, 1995.

ROTATIONALLY DISORDERED ILLITE/SMECTITE IN PALEOZOIC K-BENTONITES

DOUGLAS K. MCCARTY AND R. C. REYNOLDS JR.

Department of Earth Sciences, Dartmouth College, Hanover, New Hampshire 03755

Abstract—The three-dimensional crystal structure of rotationally disordered illite/smectite (I/S) in K-bentonite samples from the Appalachian basin and neighboring areas is described using the parameters of 1) P_0, the proportion of zero-degree layer stacking rotations, such as in the polytype series *1Md-1M*; 2) P_{cv}, the proportion of 2:1 layers with *cis*-vacant (*cv*) octahedral sites that are randomly interstratified with *trans*-vacant (*tv*) layers; and 3) P_{60}, the proportion of layers with $n \cdot 60°$ rotations (as opposed to $n \cdot 120°$) in the rotated layers. These parameters were determined by computer modeling of experimental randomly oriented powder X-ray diffraction patterns.

The proportion of *cv* interstratification in the I/S increases with Al and decreases with Mg and Fe content. The proportion of $n \cdot 60°$ rotations in the rotated layers increases with Mg and Fe content. The *cv* 120° disordered structure correlates with tetrahedral Al for Si substitution and increasing tetrahedral charge. The *tv* $n \cdot 60°$ disordered structures correlate with octahedral Mg for Al substitution. The data indicate that the type of unit cell and nature of rotational disorder in I/S is controlled by the octahedral Mg content. The three-dimensional structures do not show any systematic correlation with Reichweite and percent expandability as determined from diffraction patterns of oriented sample preparations.

Key Words—Bentonite, *Cis*-vacant octahedra, Crystal structure, Illite/Smectite, Polytype, Rotational disorder, X-ray diffraction.

INTRODUCTION

A number of papers describe the calculation of three-dimensional powder X-ray diffraction patterns of phyllosilicates with various kinds and amounts of disorder (e.g., Plançon and Tchoubar 1977a, 1977b, Plançon 1981, Plançon *et al* 1988, Drits *et al* 1984, Sakharov *et al* 1990). The book by Drits and Tchoubar (1990) is a comprehensive state-of-the-art treatment of the subject. Reynolds (1993) developed a computer algorithm (WILDFIRE) similar to those described above for calculating three-dimensional powder diffraction patterns of illite and mixed-layer illite smectite (I/S) with various types and quantities of rotational disorder. This computer program was used to model diffraction patterns of I/S separated from 56 K-bentonite samples in and around the Appalachian basin (Figure 1), thus quantifying the type and amount of crystallographic disorder in each sample. Such disordered I/S structures would have previously been called simply *1Md* polytypes using routine analytical methods. The goals of this study were to accurately model and characterize the three-dimensional I/S structures and to correlate compositional trends with the type of layer rotations and the distribution of octahedral cations.

An important distinction is made between 1) rotational disorder which refers to the angular displacements between the $-X$ direction of two adjacent unit cells stacked along c and 2) Reichweite which describes the random or ordered stacking sequences of different kinds of phyllosilicate layers along Z in a MacEwan crystallite. In this paper the term disorder refers to rotational disorder unless otherwise specified.

Early work on illite polytypes by Maxwell and Hower (1967) recognized a general transformation from *1Md* to a *2M* structure which was complete when temperatures reached the biotite isograd. Experimental work with muscovite compositions indicated the general transformation *1Md* → *1M* → *2M*$_1$ with increasing temperature (Yoder and Eugster 1955, Velde 1965). Work by Radoslovich and Norrish (1962) and Güven (1971) indicated that compositional variations affect what mica polytype results under given physical conditions.

The 2:1 layers in the usual dioctahedral mica structure have vacant M1 (*trans*) octahedra, whereas both the M2 (*cis*) octahedral sites are occupied (Figure 2). This *trans*-site vacancy and cation arrangement results in the mirror plane symmetry characteristic of the *C2/m* space group. The existence of 2:1 phyllosilicates with different distributions of octahedral cations was first reported by Méring and Oberlin (1967) for a sample of Wyoming montmorillonite. Oblique texture electron diffraction (OTED) work by Tsipursky and Drits (1984) showed that dioctahedral smectites have a wide range of octahedral cation distributions over *trans* and *cis* sites. The *trans*-occupied (*cis*-vacant) unit cell is noncentrosymmetric and belongs to space group *C2* (Tsipursky and Drits 1984) rather than *C2/m*, which applies to the *trans*-vacant structure.

Specific distortions of *cis* and *trans* octahedra result from the distribution of the octahedral cations and the

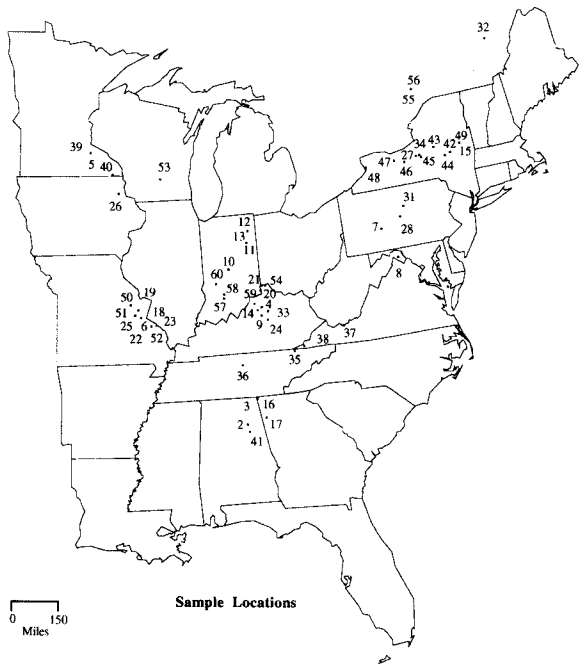

Figure 1. Sample locations and numbers.

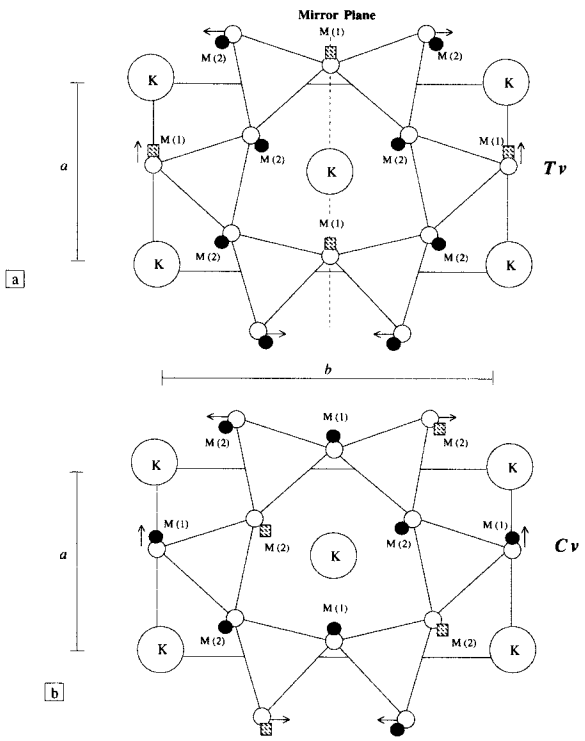

Figure 2. Diagrammatic projection of (a) *trans*-vacant I/S structure; (b) *cis*-vacant I/S structure. Arrows show direction of tetrahedral rotation, solid circles are filled octahedral sites, boxes are vacant sites.

resulting electrostatic forces. In the centrosymmetric 2:1 layer the larger vacant *trans* octahedral site causes the center of the ditrigonal ring of the top tetrahedral sheet to be shifted from the center of the bottom tetrahedral sheet by more than the ideal $-a/3$ value. This type of distortion for Al, Mg micaceous 2:1 phyllosilicates leads to a monoclinic angle (β) of about 101.3° (Bailey 1984, Drits *et al* 1993, Reynolds and Thomson 1993). In the noncentrosymmetric 2:1 layer there is an undershift of the top tetrahedral sheet resulting in β = 99.13° (Tsipursky and Drits 1984, Drits *et al* 1984, 1993). Diffraction effects are different for *cis*- and *trans*-vacant structures, for interstratification of layers with vacant *cis* and *trans* sites, and also for structures with a statistical distribution of cations between *cis* and *trans* sites within single layers (Tsipursky and Drits 1984, Drits *et al* 1984, 1993).

Experimental work by Reynolds (1992) showed that *d*(*hkl*) is independent of the average crystal thickness in the *c* direction for a mixed-layered I/S and there is no three-dimensional coherence across the expandable interfaces that separate illite layers or stacks of thin illite packets. A randomly oriented preparation of I/S diffracts in three dimensions like a randomly oriented powder of thin illite crystals. Reynolds (1993) demonstrated that *cis*-vacant (*cv*) structures exist in I/S exhibiting the *1M* and *1Md* stacking sequences, and that *cv* 2:1 layers can be interstratified with *trans*-vacant (*tv*) 2:1 layers. Reynolds (1993) also demonstrated that the computer program WILDFIRE can successfully model random powder diffraction patterns and quantify the percent of *cis*- and *trans*-vacant octahedral sites along with the percent and degree of rotational disorder. Such crystallographic characterization has been accomplished for I/S from the Ordovician and Devonian bentonite beds in and around the Appalachian basin and is the subject of this study.

Clay separations from Appalachian basin Ordovician and Devonian K-bentonites were chosen for this study because I/S from K-bentonites are better suited to show the diffraction effects produced by different types and percentages of disorder and octahedral cation distributions than are I/S from shales and sandstones which almost always have diffraction peak interferences from other fine-grained minerals.

GEOLOGIC SETTING

K-bentonites

Ordovician volcanic ash layers deposited in epeiric seas presently cover about 1.3 million km^2 of eastern North America, distributed throughout thick sequences of carbonate and clastic rocks (Kolata *et al* 1984). Most of the Ordovician K-bentonite samples in this study were collected from the Deicke and Millbrig and stratigraphic equivalent beds (Kolata *et al* 1984), the

Black River Group (Johnsson 1984), and the Utica Formation (Mitchell 1992).

The Tioga Bentonite is the best known and most wide-spread volcanic ash layer in the middle Devonian rocks of the Appalachian basin and probably covered all of the northeastern United States during middle Devonian time (Dennison and Textoris 1970, Droste and Vitiliano 1973). The Devonian K-bentonite samples in this study are from the Tioga or Tioga equivalent bentonite beds.

Post-deposition

A number of workers have suggested a "fluid migration hypothesis" to explain post-depositional features in the Appalachian basin (e.g., Oliver 1986, Hearn *et al* 1987, Bethke and Marshak 1990). For example, I/S diagenesis in the distal Appalachian basin cannot be explained by the "traditional" model of burial diagenesis (e.g., Perry and Hower 1970, Hower *et al* 1976, Jennings and Thompson 1986, McCarty and Thompson 1991) because conodont alteration index (CAI) values are too low (Harris 1979), and apparent burial depths too shallow. Yet, the I/S clays in Appalachian basin K-bentonites are $R \geq 1$ structures with low to medium expandability similar to those found in deeply buried diagenetic sequences, and most of these clays occur in geologic areas which show no evidence of being subjected to the burial conditions and associated temperatures that are considered necessary to produce this type of I/S (Huff and Türkmenoglu 1981, Elliott and Aronson 1987).

The I/S in the K-bentonite beds from the Cincinnati Arch area contain about 70 to 80% illite layers (Huff and Türkmenoglu 1981, Elliott and Aronson 1993, results from this study). The maximum burial temperatures near 80°C (Harris 1979) appear to be less than the minimum temperature of about 100°C proposed by Hower *et al* (1976) which is needed to form ordered I/S of this type. Many of the K-bentonites are enclosed in carbonate strata which could not have provided potassium, so an external source is indicated but not known. Roden *et al* (1992, 1993) found partially annealed zircon fission tracks throughout the southern Appalachian basin indicating temperatures of about 175°C that lasted less than 1 m.y. This temperature is higher than the regional CAI (about 80°C). Roden *et al* (1993) suggest that fluid flow was apparently localized in or near the K-bentonites, partially annealing zircon fission tracks, completely annealing apatite fission tracks, but not affecting conodont alteration indices on a regional scale.

ANALYTICAL METHODS

Sampling

Figure 1 shows the locations of the 56 K-bentonites used in this study (their approximate geographic coordinates are included in Table 1). Eight K-bentonites were collected from core (samples: 11–13 and 57–60) and the rest collected from outcrops. Samples 6, 22, 23, 25 were collected by the authors and all others were obtained from colleagues.

Random powder preparation

Samples were lightly crushed in an Alundum mortar and disaggregated in distilled water with an ultrasonic probe. The <1.0-μm (equivalent spherical diameter) and/or <0.5-μm size fractions were separated by timed centrifugation. Clay suspensions were saturated with 1 M $CaCl_2$ to induce flocculation to aid in collection and to exchange interlayer cations with a common ion in order to maintain comparable expandability measurements between the samples. All samples were subsequently washed repeatedly to remove excess chloride until the discarded wash showed no evidence of chloride when tested with $AgNO_3$. Washed samples were concentrated by ultracentrifugation. The core samples were obtained as clay separates and their preparation is described by Elliott and Aronson (1987).

All clay separates were redispersed in 50 ml of distilled water for freeze-drying. The suspensions were frozen in a Labconco shell freezer at −30°C and lyophilized in a Labconco 4.5 freeze drier. The freeze-dried clay was ground lightly with a rubber stopper mounted on a glass rod. Immediately prior to XRD analysis, the freeze-dried outcrop separates were dehydrated in an oven at either 250°C or 350°C for one h. The core sample separations were spread in an evaporating dish and solvated with ethylene glycol vapor for 24 h at 60°C before preparing a random powder X-ray diffraction (XRD) mount. The core separates were treated with ethylene glycol solvation instead of heating because they were to be used in a future study for which heating was inappropriate. All randomly oriented sample mounts were prepared for XRD by a side-loading method using a sample holder 3 cm long, 2.35 cm wide, and 0.15 cm deep that accommodates approximately 600 mg of clay.

Orientated aggregate preparation

Oriented XRD preparations were made by dispersing approximately 200 mg of clay separate in 2 ml of water, pipetting the suspension onto a glass slide, and drying at room temperature. Oriented XRD mounts were analyzed air-dried and after vapor solvation with ethylene glycol at 60°C for 12 h.

X-ray diffraction analysis

Diffraction data were collected with a Siemans D-500 diffractometer equipped with a digital step counter, a diffracted beam graphite monochromator, 1° beam and 0.15° detector slits and using CuKα radiation. All step scans were conducted at 2θ increments of 0.05°. Count times for the random powder preparations were 20 s per step and runs were made from 16–44 °2θ. Runs for

Table 1. Sample locations and structural parameters.

Decimal long.	Decimal lat.	Sample #	Bentonite bed and location	Exp. %	Reic.	P_0	P_{cv}	P_{60}
−86.00	34.00	2	Deicke AL	11	3	50	25	70
−86.00	34.00	3	Deicke AL	18	1.5	75	30	85
−85.00	38.20	4	Deicke KY	21	1	50	80	60
−92.70	44.42	5	Deicke MN	22	1	45	60	60
−90.53	38.25	6	Deicke MO	29	1	60	60	50
−78.50	40.58	7	Ordovician PA	11	3	70	82	30
−78.00	39.45	8	Deicke W.VA	11	3	80	60	30
−84.85	38.00	9	Ordovician KY	18	1.5	70	75	20
−86.17	39.83	10	Ordovician IN	21	1	65	60	25
−85.20	40.75	11	Ordovician IN	16	3	70	75	35
−85.08	41.17	12	Ordovician IN	13	3	55	60	60
−85.08	41.17	13	Ordovician IN	22	1.5	60	85	20
−84.80	38.30	14	Ordovician KY	24	1	70	70	40
−73.83	43.13	15	Ordovician NY	18	1	60	65	40
−85.45	34.92	16	Millbrig GA	14	3	85	55	60
−85.10	34.20	17	Deicke GA	9	3	65	40	90
−90.53	38.25	18	Deicke MO	26	1	50	50	50
−90.63	38.53	19	Millbrig MO	27	1	50	50	50
−84.72	38.93	20	Deicke KY	29	1	55	85	60
−84.67	39.12	21	Ordovician KY	15	2.5	75	50	75
−90.53	38.25	22	Millbrig MO	27	1	60	65	65
−90.53	38.25	23	Millbrig MO	27	1	60	60	45
−84.58	37.83	24	Millbrig KY	26	1	60	60	65
−90.53	38.25	25	Deicke MO	19	1	50	60	60
−91.33	42.87	26	Nasset Ord. IA	15	3	75	35	95
−76.00	43.00	27	Ordovician NY	18	1.5	62	75	45
−77.50	40.90	28	Ordovician PA	14	2.5	75	60	40
−77.25	41.25	31	Ordovician PA	12	3	60	80	25
−71.25	46.75	32	Ordovician Quebec	26	1	50	90	20
−84.53	38.15	33	Ordovician KY	15	3	45	55	60
−76.17	42.97	34	Tioga NY	10	3	60	80	35
−83.47	36.57	35	Deicke TN	10	3	50	30	60
−85.92	36.25	36	Deicke TN	30	1	65	75	46
−81.08	37.25	37	Deicke VA	9	3	50	30	80
−83.00	36.70	38	Deicke VA	13	2.5	85	35	90
−92.70	44.42	39	Deicke MN	26	1	60	60	45
−91.60	43.58	40	Millbrig MN	27	1	30	90	35
−85.92	33.70	41	Millbrig AL	11	3	70	55	60
−74.42	42.88	42	Ordovician NY	19	2.5	55	85	30
−75.17	43.17	43	Ordovician NY	11	3	45	65	45
−74.70	42.78	44	Tioga NY	13	3	55	75	15
−75.92	42.92	45	Tioga NY	13	3	50	98	20
−76.78	42.85	46	Tioga NY	9	3	50	85	10
−77.27	42.93	47	Tioga NY	12	3	55	97	15
−78.73	42.88	48	Tioga NY	21	1.5	55	80	45
−73.83	43.13	49	Ordovician NY	18	1.5	55	85	10
−91.00	38.72	50	Millbrig MO	33	1	50	50	50
−90.83	38.35	51	Deicke MO	29	1	50	50	65
−90.08	37.92	52	Deicke MO	31	1	60	50	50
−89.20	43.33	53	Ordovician WI	19	1.5	65	45	75
−84.50	39.08	54	Deicke KY	15	2.5	50	90	45
−75.67	45.50	55	Ordovician Ottawa	13	2.5	70	60	40
−75.67	45.50	56	Ordovician Ottawa	21	2.5	50	95	35
−86.50	38.75	57	Ordovician IN	24	1	60	95	30
−86.50	38.92	58	Ordovician IN	22	1	70	80	25
−85.13	38.47	59	Ordovician KY	26	1	60	90	30
−86.83	39.33	60	Ordovician IN	19	1.5	45	92	40
Min.				9	1	30	25	10
Max.				33	3	85	98	95
Average				19	2	59	66	47

the oriented preparations were made at 1 to 5 s per step from 2–50 °2θ. These conditions produced a peak height intensity of approximately 10,000 counts for the mica prism reflection near 19.9 °2θ (the 020;110).

I/S expandability and Reichweite determinations were made from the oriented aggregate diffraction patterns using the delta-2θ method described in Moore and Reynolds (1989) and in some cases by means of the NEWMOD computer program (Reynolds 1985).

Computer modeling of three-dimensional structures

The three-dimensional structural parameters of percent *cv*, percent *tv*, and the percent and type of rotational disorder in the I/S were determined by modeling each diffraction pattern with the computer program WILDFIRE (Reynolds 1993). No attempt is made here to describe the WILDFIRE algorithm and the reader is referred to Reynolds (1993) for a complete description.

All of the calculated diffraction profiles are based on atomic coordinates and unit cell parameters for *cv* and *tv* unit cells from Tsipursky and Drits (1984) and Drits *et al* (1984). The *cv* unit cell dimensions are: a = 5.199 Å, b = 9.005 Å, c = 10.09 Å and β = 99.13°. The *tv* unit cell dimensions are: a = 5.199 Å, b = 9.005 Å, c = 10.164 Å and β = 101.3°. In every case the calculated diffraction patterns were based on crystals containing 60 unit cells along X and 30 unit cells along Y. Crystal size in the Z direction was determined on a case by case basis as part of the WILDFIRE modeling procedure. The number of unit cells in the Z direction depends on a particle size distribution that is calculated from I/S expandability and Reichweite (see also Altaner and Bethke 1988). Particle size distributions used in the calculated diffraction patterns that are shown later as examples are presented in Table 2. Fe and K were not varied in any of the calculated diffraction patterns from the default values of 0.14 and 0.7 atom per formula unit, respectively. Composition, atomic coordinates, and crystal dimensions in X and Y were not varied in WILDFIRE, and the particle thickness distribution was estimated from basal diffraction data. Therefore, all of the diffraction patterns in this study were modeled with combinations of just three adjustable input parameters P_{cv}, P_0, and P_{60}. P_{cv} refers to the percentage of *cv* layers interstratified with *tv* layers in the calculated model crystallite structure where:

$$P_{cv} + P_{tv} = 100.$$

P_0 is the percentage of layers rotated zero degrees with respect to a preceding adjacent layer. P_0 = 100% describes the *1M* polytype where all layers have the same orientation. For structures with rotational disorder of type $n\cdot 120°$, $P_{120°} = P_{240°}$. If P_0 = 33% there are equal proportions of interlayers involving 0°, 120°, and 240° rotations of adjacent layers. P_0 = 33% produces the greatest amount of disorder or highest degree of "*1Md*-ness" possible. If $P_0 < 33\%$ then the structure is partially ordered with respect to the 120° and 240° rotations, as are $2M_1$ and *3T* structures. This latter type of nearest-neighbor or next-nearest neighbor ordering does not pertain to any of the samples or modeled structures in this study.

Table 2. Crystallite thickness distribution for calculated patterns shown in Figures 5–10.

	Sample					
N^1	34 Tioga NY	8 Deicke W.VA	45 Tioga NY	26 Nasset IA	18 Deicke MO	40 Millbrig MN
1	0	0	0	0	0	0
2	0.067	0.067	0.067	0.272	0.512	0.422
3	0.188	0.188	0.188	0.228	0.269	0.268
4	0.285	0.285	0.285	0.217	0.129	0.161
5	0.193	0.193	0.193	0.140	0.55	0.081
6	0.129	0.129	0.129	0.88	0.023	0.04
7	0.084	0.084	0.084	0.055		
8	0.054	0.054	0.054			

N^1 is the number of 2:1 layers per crystallite.

Rotations of $n\cdot 60°$ (n = odd integer) are possible and are not crystallographically equivalent to rotations of $n\cdot 120°$, but rotations of 60°, 180°, and 300° are crystallographically equivalent to each other. P_{60} refers to the proportion of layers that are rotated $n\cdot 60°$ out of the total fraction of rotated layers (P_0 not being considered a rotated layer). If P_{60} = 0 all of the rotational disorder is of the $n\cdot 120°$ type. If P_{60} = 100% rotations of 120° and 240° are eliminated, producing a random stacking sequence of 60°, 180°, and 300° rotations. When P_{60} = 60% there are equal proportions of 60°, 120°, 180°, 240°, and 300° rotations.

Intensities of diffraction peaks from the experimental random powder diffraction patterns are affected by preferred orientation of the clay powder in the sample holder. The calculated patterns are compensated for this effect by means of the March function correction factor (Dolasse 1986). A correction factor of 1.0 describes perfect random orientation. Correction factors of less than 1.0 simulate the effects of preferred orientation where proportionally more crystals in the aggregate mount are oriented with d(001) parallel to the surface of the mount. A correction factor was obtained by measuring departures of the 003/(020,110) intensity ratios from the values calculated for random orientations.

WILDFIRE calculates basal reflections separately and adds them to the three-dimensional calculated reflections after normalizing for absolute intensity and preferred orientation. Special attention was paid to modeling the basal reflection part of the composite three-dimensional calculations by first modeling the basal part of the measured random diffraction patterns with NEWMOD (Reynolds 1985) and then using the de-

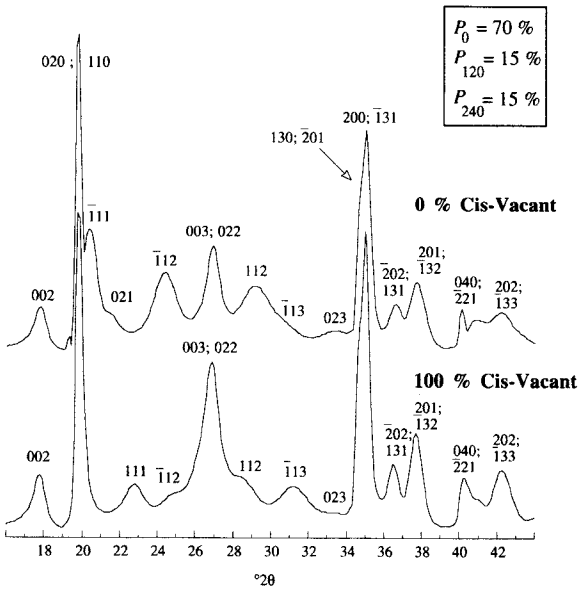

Figure 3. Calculated diffraction patterns for 0% *cv* and 100% *cv* structures. The parameters are: P_0 = 70% and all rotated layers are $n\cdot120°$ (P_{120} = 15%; P_{240} = 15%; P_{60} = 0) in both calculations.

termined 00*l* parameters in the WILDFIRE calculations. The basal reflections contain no information about three-dimensional disorder and the octahedral cation distributions. They are included here to model correctly interferences between three-dimensional and basal reflections.

Diffraction pattern interpretation

The diagnostic *hkl* reflections used to determine P_{cv} and P_0, and the unit-cell type of a mica polytype are of the category $k \neq 3n$. These peaks, and all *hkl* reflections, are broadened by small crystal size and/or rotational disorder. To extract model P_{cv} and P_0 values requires an analysis of the 02*l*; 11*l* reflections between 19 and 34 °2θ. The region between 34 and 39 °2θ consists of the $k = 3n$ reflections 20*l*; 13*l* and is useful for determining the quantity of $n\cdot60°$ rotations, P_{60}. Both $n\cdot60°$ and $n\cdot120°$ rotations have very similar effects on the 02*l*; 11*l* peaks (Drits *et al* 1984, Sakharov *et al* 1990, Drits and Tchoubar 1990, Reynolds 1993, this study). Modeling of experimental diffraction patterns with WILDFIRE consists of adjusting the input parameters P_0, P_{cv}, and P_{60} until agreements of peak position (*d*-value) and peak shape are optimized between the experimental and the calculated diffraction patterns.

Figure 3 illustrates the differences between a disordered *tv* I/S (*1Md*) and a disordered *cv* I/S (*1Md*). Both of these calculated patterns have P_0 = 70% and the rotations of the remaining 30% of layers are of the $n\cdot120°$ type. The *hkl* indices of diagnostic peaks are shown on the figure; Reynolds (1993) discussed the details of the peak positions and relative intensities.

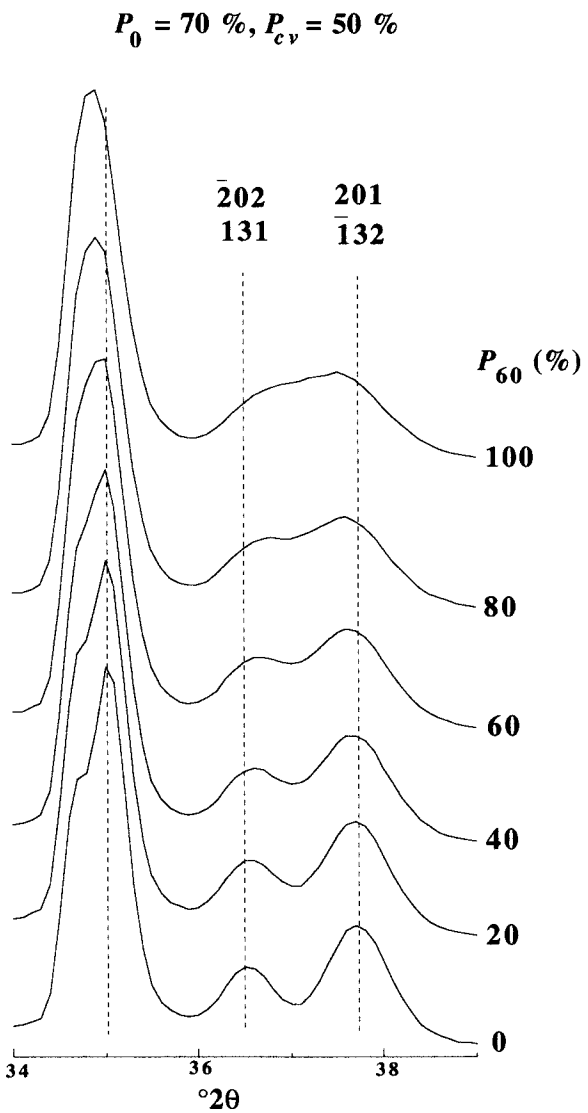

Figure 4. Calculated diffraction patterns demonstrating the effects of $n\cdot60°$ rotational disorder on the 20*l*; 13*l* reflections. The parameters are: P_0 = 70%, and P_{cv} = 50% for all of the calculations.

Figure 4 illustrates the effect of increasing values of P_{60} on the 20*l*; 13*l* reflections. The calculations in Figure 4 were all made with P_0 = 70%, P_{cv} = 50%, and the P_{60} values shown on the figure. P_{60} values are the fraction of the 30% of rotated layers that consist of equal proportions of 60°, 180°, or 300° rotations. These calculations show the migration of the $\bar{2}02$; 131 and 201; $\bar{1}32$ reflections toward each other so that when all of the rotated layers are of the $n\cdot60$ type there is a single broad peak at about 37 °2θ.

Table 3. Chemical analyses.

Sample Units:	SiO_2 %	Al_2O_3 %	Fe_2O_3 %	MgO %	CaO %	Na_2O %	K_2O %	P_2O_5 %	TiO_2 %	Cr_2O_3 %	MnO %	F PPM	Rb PPM	Sr PPM	Y PPM	Zr PPM	Nb PPM	Ba PPM	LOI %	SUM %
41 Millbrig AL	52.9	24	3.14	3.47	1.68	−0.01	6.58	1.15	0.342	−0.01	−0.01	2800	168	332	989	383	16	−10	7.3	100.7
55 Ordov. Ottawa	53.8	25.2	0.84	3.93	1.97	−0.01	6.49	1.25	0.085	−0.01	−0.01	4790	199	391	10	80	−10	−10	7	100.6
56 Ordov. Ottawa	53	29.2	1.25	2.5	1.45	−0.01	4.81	0.19	0.216	−0.01	0.01	3050	156	354	16	126	−10	14	8.05	100.8
42 Ordov. NY	51.8	29.6	2.01	2.2	1.11	−0.01	5.3	0.27	0.161	−0.01	−0.01	1380	142	251	10	127	−10	95	8	100.5
7 Ordov.PA	52.4	27.6	1.6	3.44	0.84	−0.01	5.98	0.38	0.148	−0.01	−0.01	6670	190	13	30	72	−10	396	8.15	100.6
8 Deicke W.VA	51	29.6	1	2.47	1	−0.01	5.67	0.76	0.129	−0.01	−0.01	2310	202	11	18	110	−10	4800	8.55	100.8
49 Ordov. NY	52.3	27.1	2.5	2.79	1.16	−0.01	5.2	0.41	0.157	−0.01	−0.01	2250	152	27	27	264	−10	57	9.05	100.7
16 Millbrig GA	54.4	23.4	3.64	4.19	1.04	−0.01	6.18	0.13	0.234	−0.01	−0.01	3940	159	−10	31	272	12	−10	7.6	100.9
17 Deicke GA	54.1	23	3.67	3.42	1.5	−0.01	4.92	1.21	0.291	−0.01	−0.01	2670	117	−10	107	56	−10	−10	8.75	100.9
18 Deicke MO	52.9	23.4	2.91	3.89	2.12	−0.01	5.35	0.81	0.249	−0.01	−0.01	6210	204	389	14	178	−10	−10	8.7	100.4
19 Millbrig MO	52.8	22.9	1.24	3.92	2.63	−0.01	5.56	1.58	0.255	−0.01	−0.01	5420	177	544	−10	95	−10	−10	9.4	100.4
21 Ordov. KY	53.8	20.1	1.35	4.72	3.95	−0.01	5.32	3.46	0.241	−0.01	−0.01	8000	145	37	15	116	−10	−10	7.55	100.5
24 Millbrig KY	54.7	22.1	1.23	4.37	2.12	−0.01	5.5	1.32	0.138	−0.01	−0.01	6100	140	25	11	78	14	−10	9	100.5
40 Millbrig MN	53.3	23.8	2	3.61	1.89	−0.01	5.68	0.54	0.246	−0.01	0.02	3450	141	348	−10	132	−10	−10	9.3	100.5
26 Nasset IA	55.2	20.6	1.27	5.94	1.88	−0.01	6.35	1.21	0.219	−0.01	−0.01	6760	153	400	−10	147	16	−10	7.55	100.3
27 Ordov. NY	53.4	28.5	1.69	2.34	0.98	−0.01	4.78	0.31	0.229	−0.01	−0.01	1830	132	30	28	174	−10	972	8.05	100.3
53 Ordov. WI	51.4	20.6	2.36	4.55	3.37	−0.01	5.71	2.63	0.196	−0.01	0.01	5110	126	631	13	332	−10	−10	9.6	100.6
34 Tioga NY	54	24.3	1.28	4.14	0.88	−0.01	6.7	0.5	0.153	−0.01	−0.01	8040	172	−10	−10	54	−10	21	8.45	100.4
39 Deicke MN	53.6	23.9	1.48	3.41	1.91	−0.01	5.14	0.75	0.308	−0.01	−0.01	2690	99	13	12	203	−10	−10	10	100.5
45 Tioga NY	51.9	24.5	0.98	3.56	3.18	−0.01	6.53	2.16	0.19	−0.01	0.01	8280	200	578	−10	59	−10	−10	7.15	100.3
3 Deicke AL	55.8	21.8	2.94	5.22	0.77	−0.01	6.43	0.15	0.377	−0.01	−0.01	4600	147	123	−10	49	−10	−10	6.85	100.4

Table 4. Structural formulae.

Sample	Units	Inter-layer K atoms	Inter-layer Ca atoms	Tet. Si atoms	Tet. Al atoms	Oct. Al atoms	Oct. Fe atoms	Oct. Mg atoms	Oct. cation sum atoms	Tet. charge	Oct. charge	2:1 charge	Inter-layer charge
41 Millbrig	AL	0.57	0.12	3.57	0.43	1.48	0.16	0.35	1.99	−0.43	−0.38	−0.81	0.81
55 Ordov.	Ottawa	0.67	0.15	3.37	0.63	1.52	0.08	0.42	2.02	−0.63	−0.34	−0.97	0.97
56 Ordov.	Ottawa	0.49	0.12	3.27	0.73	1.71	0.12	0.26	2.09	−0.73	0.03	−0.7	0.73
42 Ordov.	NY	0.54	0.08	3.2	0.8	1.68	0.2	0.23	2.11	−0.8	0.1	−0.71	0.70
7 Ordov.	PA	0.61	0.06	3.26	0.74	1.6	0.16	0.36	2.12	−0.74	−0.003	−0.74	0.73
8 Deicke	W.VA	0.59	0.08	3.21	0.79	1.74	0.1	0.26	2.1	−0.79	0.05	−0.74	0.75
49 Ordov.	NY	0.54	0.09	3.26	0.74	1.56	0.25	0.3	2.11	−0.74	0.03	−0.71	0.72
16 Millbrig	GA	0.63	0.08	3.35	0.65	1.31	0.36	0.44	2.11	−0.65	−0.13	−0.78	0.79
17 Deicke	GA	0.51	0.11	3.39	0.61	1.35	0.37	0.36	2.08	−0.61	−0.13	−0.74	0.73
18 Deicke	MO	0.56	0.16	3.34	0.66	1.35	0.29	0.42	2.06	−0.66	−0.22	−0.88	0.88
40 Millbrig	MN	0.6	0.14	3.39	0.61	1.45	0.2	0.39	2.04	−0.61	−0.27	−0.89	0.88
27 Ordov.	NY	0.49	0.07	3.3	0.7	1.69	0.17	0.24	2.1	−0.7	0.07	−0.63	0.63
34 Tioga	NY	0.7	0.07	3.41	0.59	1.49	0.13	0.44	2.06	−0.59	−0.24	−0.83	0.84
39 Deicke	MN	0.54	0.15	3.43	0.57	1.51	0.15	0.37	2.03	−0.57	−0.27	−0.84	0.84
3 Deicke	AL	0.65	0.06	3.44	0.56	1.27	0.29	0.55	2.11	−0.56	−0.21	−0.77	0.77
26 Nasset	IA	0.67	0.14	3.51	0.49	1.29	0.13	0.64	2.06	−0.49	−0.46	−0.95	0.95
24 Millbrig	KY	0.58	0.16	3.5	0.5	1.42	0.13	0.48	2.03	−0.5	−0.41	−0.91	0.90
19 Millbrig	MO	0.59	0.2	3.42	0.58	1.44	0.13	0.43	2	−0.58	−0.43	−1.01	0.99
53 Ordov.	WI	0.62	0.27	3.39	0.61	1.23	0.25	0.51	1.99	−0.61	−0.54	−1.16	1.16
45 Tioga	NY	0.69	0.25	3.33	0.67	1.47	0.1	0.39	1.96	−0.67	−0.51	−1.18	1.19
21 Ordov.	KY	0.57	0.31	3.5	0.5	1.28	0.14	0.52	1.94	−0.5	−0.69	−1.19	1.19

Chemical analysis

Bulk chemical analyses were made by X-ray fluorescence methods (XRF) on 21 clay-fraction separations (Table 3) by X-ray Assay Laboratories, Don Mills, Ontario. These samples were chosen on the basis of 1) structural diversity after XRD and WILDFIRE modeling, 2) geographic distribution, and 3) adequate sample size (1.5 g). Each separate sent for XRF analysis was checked for contamination by random-powder XRD analysis.

RESULTS

Chemical composition

Table 3 shows chemical analyses and Table 4 shows calculated I/S structural formulae based on an $O_{10}(OH)_2$ formula unit. Total Fe was calculated as Fe^{3+}. Samples 19, 53, 45 and 21 all have anomalously high 2:1 layer charges. This high layer charge may be due to small amounts of secondary mineral phase(s), based on closer inspection of the random powder diffractograms from the separates submitted for analysis. These samples were not used in subsequent structure-composition correlation.

X-ray diffraction and modeling

Table 1 lists sample name and location (Figure 1), along with the I/S structural parameters of percent expandability, Reichweite determined from oriented-sample XRD and NEWMOD modeling, and the parameters P_0, P_{cv}, and P_{60} determined from modeling each random diffraction pattern with WILDFIRE. There is greater uncertainty in accuracy of the P_{60} parameter than there is for P_0 and P_{cv}, because the $20l$; $13l$ diffraction profile used to model P_{60} is also affected by crystal shape, Fe content, and tetrahedral tilt and rotation (Reynolds 1993).

P_{cv} is less accurate if P_0 is low. If P_0 is near the lower limit of 33% the diagnostic $k \neq 3n$ reflections are so broad that a large change in the P_{cv} input parameter has little or no visible change in the calculated diffraction pattern. When P_0 values increase and the $k \neq 3n$ reflections become better resolved, the accuracy of the corresponding P_{cv} values increases. The nature of rotational stacking defects and their effect on peak position and the accuracy of *cv* determination are examined in detail by Drits and McCarty (1995).

Figures 5–10 show random-powder diffraction patterns of dehydrated I/S along with their corresponding WILDFIRE calculated patterns. They are presented as examples that show a range of the modeled P_0, P_{cv}, and P_{60} parameters and are representative of all of the samples and corresponding calculated patterns. The comparisons demonstrate the utility of calculated patterns in realistically modeling three-dimensional I/S crystal structures involving interstratification of *tv* and *cv* unit cells combined with different types and amounts of rotational disorder.

Dashed lines in Figures 5–10 are used to show the 2θ coincidence of the diagnostic peak positions mentioned above and shown in Figure 3. Correspondence with peak shape was made by visual inspection and achieved by trial and error adjustment of P_0, P_{cv}, and

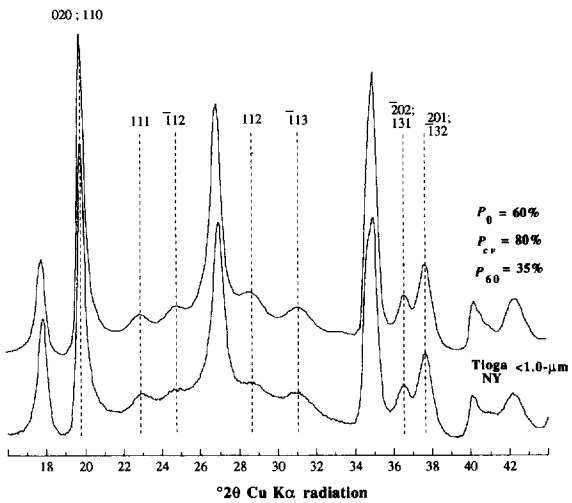

Figure 5. Comparison between calculated (top) and experimental diffraction patterns for Tioga sample 34. The parameters are: P_0 = 60%, P_{cv} = 80% and P_{60} = 35%.

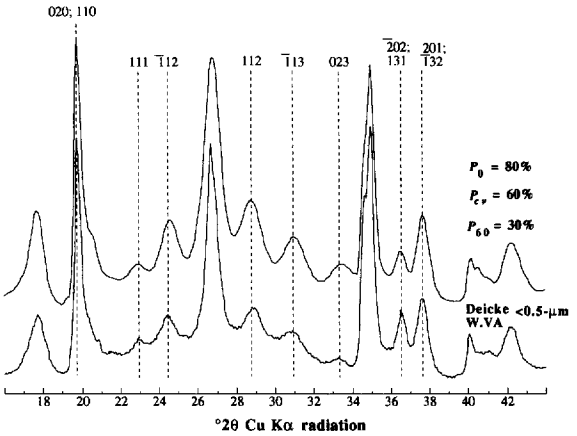

Figure 6. Comparison between calculated (top) and experimental diffraction patterns for Deicke sample 8. The parameters are: P_0 = 80%, P_{cv} = 60% and P_{60} = 30%.

P_{60}. Comparison of the *d*-values for the calculated and experimental $k \neq 3n$ reflections for the diffraction patterns in Figures 5–10 is shown in Table 5.

Figure 5 shows data for the Devonian Tioga K-bentonite, in central New York near Syracuse enclosed in the Onondaga Limestone Formation. This is an example of a good fit between a calculated and experimental diffraction pattern. The I/S has 80% *cv* interstratification, and 60% of the layers have 0° rotations. P_{60} is relatively low at 35%, indicating that the structure is dominated by $n \cdot 120°$ rotations, as evidenced by the well-modulated peaks between 36 and 39 °2θ. This Tioga sample is a "classic" example of a *1Md cis*-vacant I/S.

Sample 8 shown in Figure 6 is from the middle Ordovician Deicke K-bentonite near Martinsburg, West Virginia. This Deicke sample is a *cv*-dominated I/S comparable to the Tioga sample in Figure 5, except it is more ordered as seen by the sharper more intense $\bar{1}$12 and 112 peaks, which are also more intense because the structure has fewer *cv* layers. The diffraction pattern was modeled with P_0 = 80%, compared with P_0 = 60% for the Tioga sample, and P_{cv} is 60% in this sample compared with 80% for the Tioga. Like the Tioga I/S, this sample is dominated by $n \cdot 120°$ rotations (P_{60} = 30%).

Sample 45 shown in Figure 7 is from the Tioga K-bentonite at Jamesville, New York. It demonstrates the diffraction effects produced from a very high proportion of *cv* layers combined with a high degree of rotational disorder indicated by a P_0 value of only 50%. The $\bar{1}$12 and 112 reflections which are prominent in the *tv* structure are now just broad shoulders on both sides of the 003 peak; the 111 and $\bar{1}$13 peaks are broad, but well defined. The rotational disorder is nearly all $n \cdot 120°$ indicated by a P_{60} value of only 20%.

Sample 26 shown in Figure 8 is from the Nasset K-bentonite at Guttenberg, Iowa. This I/S is relatively well ordered with P_0 = 75%. The low P_{cv} value of 35% eliminates the 111 peak and the $\bar{1}$13 is a broad hump; at the same time the definition and intensity of both the $\bar{1}$12 and 112 peaks are enhanced. Rotations are almost all $n \cdot 60°$ as shown by the single broad peak near 37 °2θ.

Sample 18 shown in Figure 9 is from the Deicke K-bentonite in the southern Illinois basin and is very characteristic of other samples from that area. The combination of P_0, P_{cv}, and P_{60} values all equal to 50%

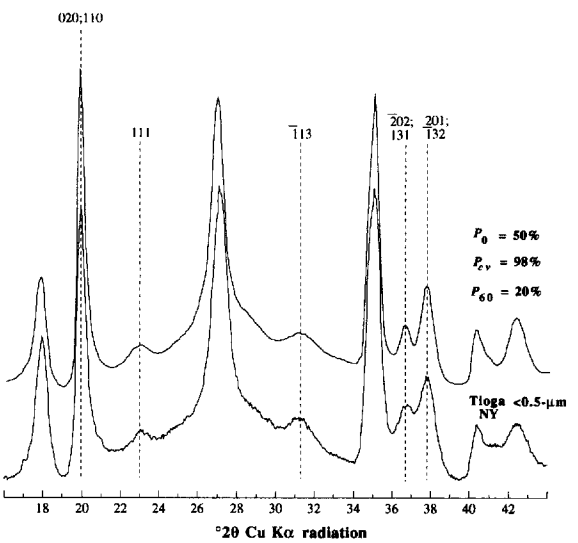

Figure 7. Comparison between calculated (top) and experimental diffraction patterns for Tioga sample 45. The parameters are: P_0 = 50%, P_{cv} = 98% and P_{60} = 20%.

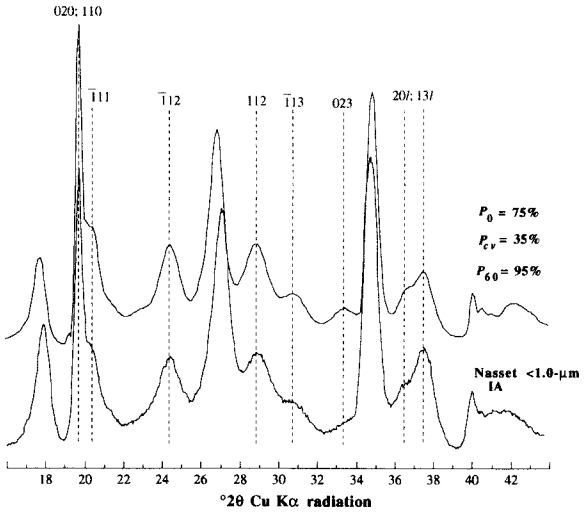

Figure 8. Comparison between calculated (top) and experimental diffraction patterns for Nasset sample 26. The parameters are: P_0 = 75%, P_{cv} = 35% and P_{60} = 95%.

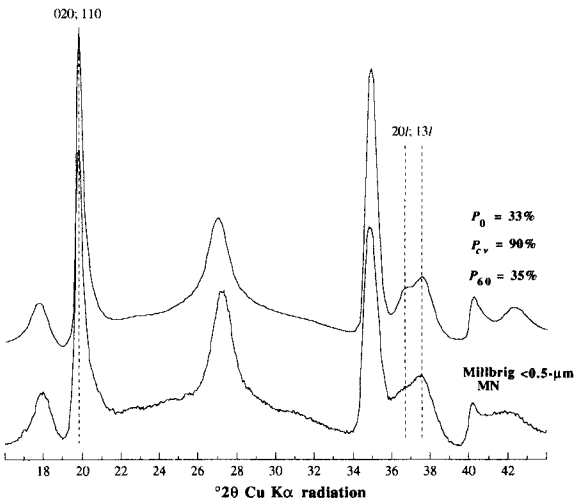

Figure 10. Comparison between calculated (top) and experimental diffraction patterns for Millbrig sample 40. The parameters are: P_0 = 30%, P_{cv} = 90% and P_{60} = 35%.

produces a unique diffraction pattern in which the $\bar{1}12$ peak is broad, but relatively well defined, and the 112 and $\bar{1}13$ peaks between 28 and 32 °2θ have merged into a broad sloping shoulder. The relatively high percentage of $n \cdot 60°$ rotations produces a single peak near 37 °2θ.

Sample 40 shown in Figure 10 is from the Millbrig K-bentonite in southeast Minnesota. P_0 is 33% indicating maximum rotational disorder, and all of the diagnostic peaks are broadened so much that they are undefined. This is an example of an end-member *1Md* structure. Large changes in P_{cv} have little visible effect on the calculated diffraction pattern and therefore the accuracy of the P_{cv} value is low.

These examples demonstrate the wide variability that exists within the general class of disordered I/S, and the power WILDFIRE has in accurately modeling I/S three-dimensional crystal structures. In some cases, such as Figure 8, the 002 and 003 peaks in the experimental diffraction pattern indicate a lower d-value than the corresponding peaks in the calculated diffraction pattern. This discrepancy suggests that the default value of $d(001)$ = 9.7 Å used for dehydrated smectite may not have been appropriate, but this quantity has no

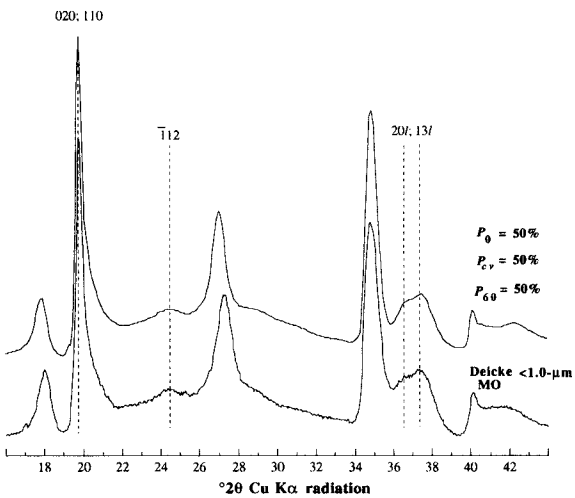

Figure 9. Comparison between calculated (top) and experimental diffraction patterns for Deicke sample 18. The parameters are: P_0 = 50%, P_{cv} = 50% and P_{60} = 50%.

Table 5.

Sample	hkl	d-value experimental (Å)	d-value calculated (Å)
34, Tioga NY	111	3.87	3.87
	$\bar{1}12$	3.60	3.59
	112	3.12	3.12
	$\bar{1}13$	2.89	2.87
8, Deicke W.VA	111	3.88	3.88
	$\bar{1}12$	3.64	3.62
	112	3.09	3.10
	$\bar{1}13$	2.90	2.88
	023	2.69	2.67
45, Tioga NY	111	3.85	3.87
	$\bar{1}13$	2.87	2.87
26, Nasset IA	$\bar{1}11$	4.38	4.34
	$\bar{1}12$	3.65	3.63
	112	3.09	3.09
	$\bar{1}13$	2.91	2.90
18, Deicke MO	$\bar{1}12$	3.65	3.63
40, Millbrig MN	—	—	—

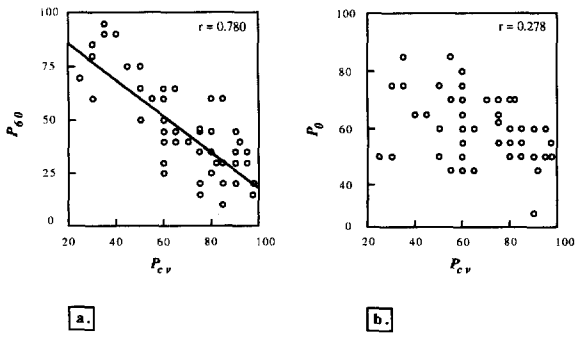

Figure 11. Structural relationships from all of the I/S samples modeled in this study: (11a) P_{cv} *vs* P_{60}; (11b) P_{cv} *vs* P_0.

effect on the positions of the diagnostic *hkl* peaks or the estimation of P_{cv}, P_0 and P_{60}.

DISCUSSION

Structure–composition relationships

Three-dimensional structural parameters. Figure 11a shows an inverse relationship between the proportion of *cv* interstratification and the proportion of $n \cdot 60°$ rotations in the rotated layers. In Figure 11b, P_{cv} is plotted against P_0 and shows no apparent relationship between the proportion of *cv* interstratification and the proportion of layers with a 0° stacking angle. The parameters P_{cv}, P_0, and P_{60} do not show any systematic correlation with I/S expandability and Reichweite.

Relationships between composition and the proportion of interstratified cis-*vacant layers.* Figure 12 shows a significant linear relationship between composition and *cv* interstratification (P_{cv}) for the I/S samples for which we have both chemical data and structural data. A decrease in *cv* interstratification correlates with an increase in Mg and Fe in I/S 2:1 layers where Mg and Fe substitute for Al in the octahedral sheets.

Layer charge relationships. Figure 13a shows a linear correlation between the increases in magnitude of both calculated octahedral charge and total 2:1 layer charge

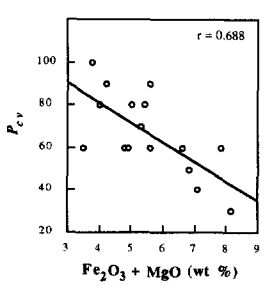

Figure 12. Relationship between composition (Fe_2O_3 + MgO) and P_{cv}.

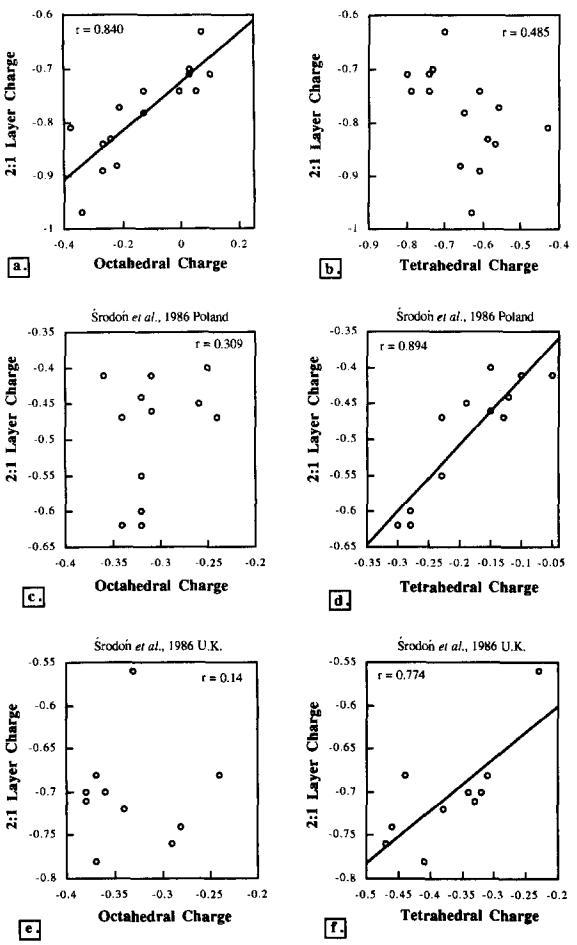

Figure 13. I/S charge relationships, calculated octahedral and tetrahedral charge *vs* calculated 2:1 layer charge. Figures (13a–b) this study. Figures (13c–d) are from Środoń *et al* (1986), a suite of I/S samples from an Upper Carboniferous bentonite Upper Silesia, Poland. Figures (13c–d) are from Środoń *et al* (1986), a suite of I/S samples from Silurian bentonites in the United Kingdom.

for the I/S samples analyzed in this study. Figure 13b shows no such systematic correlation between calculated tetrahedral charge and calculated 2:1 layer charge.

The finding that 2:1 layer charge does not have a linear relationship with tetrahedral charge is in contrast to published data for other suites of I/S samples from bentonites. Figure 13c shows octahedral charge *vs* 2:1 layer charge, and Figure 13d shows tetrahedral charge *vs* 2:1 layer charge in I/S samples from Upper Carboniferous bentonites Upper Silesia, Poland (Środoń *et al* 1986). In these samples tetrahedral charge progressively increases with 2:1 layer charge whereas no such relationship exists for octahedral and 2:1 layer charges.

Figures 13e and 13f also show no correlation be-

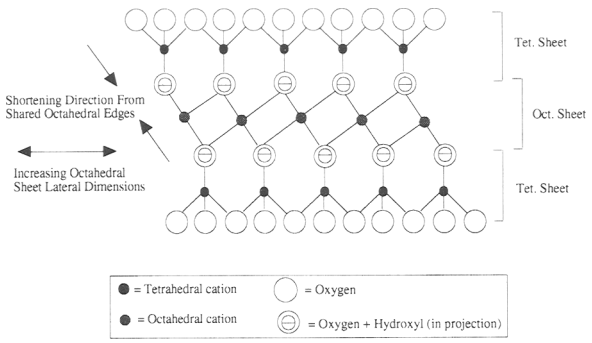

Figure 14. Side view projection of basic mica structure showing direction of shortening from shared octahedral edges and increasing octahedral sheet lateral dimensions from octahedral Mg substitution.

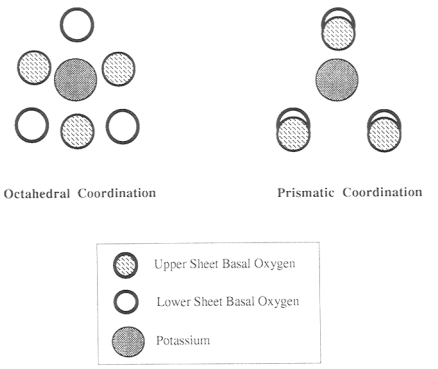

Figure 15. Basal oxygen positions in octahedral and prismatic coordination.

tween octahedral and 2:1 layer charge, but show a progressive increase in both tetrahedral charge and 2:1 layer charge in I/S samples from Silurian bentonites in the United Kingdom (Środoń *et al* 1986).

No information is available on the three-dimensional structure for the Polish or United Kingdom samples but the data suggest that the crystal chemistry of I/S may be quite different in separate geologic locations.

Crystal chemistry

In this suite of I/S samples from K-bentonites, $n\cdot 60°$ rotations are correlated with samples that have the highest content of octahedral Mg and Fe and tetrahedral Si. This observation can be reconciled by crystal chemical considerations of the basic mica structure. Tetrahedral thickening, tilt, rotation and thinning of the octahedral sheet are four mechanisms of adjustment for the misfit between the tetrahedral and octahedral sheets in the 2:1 layer. The nature and extent of these adjustments have different consequences for the subsequent rotational stacking angles in the crystal (Radoslovich 1959, Radoslovich and Norrish 1962, Bailey 1966, 1984). Shortening of shared octahedral edges in the direction diagonal to the sheet surface occurs as octahedral anions move toward each other to shield octahedral cation repulsion (Bailey 1984; Figure 14). Therefore, the entire octahedral sheet is thinned and expanded along X and Y. Lateral octahedral edges around the vacant octahedral sites are expanded as a result of this shared-edge shortening (Drits *et al* 1993, Bailey 1984). Substitution of Mg for Al in the octahedral sheet increases the lateral dimensions of the sheet. The tetrahedral sheet b-axis dimension is minimized with more Si and less Al substitution. Therefore, octahedral Mg substitution and lower tetrahedral Al reduces the misfit for a given overall 2:1 layer charge. This type of layer composition minimizes tetrahedral tilt and rotation, making a more regular structure. When misfit reduction is accomplished by tetrahedral tilting the bridging basal oxygen between adjacent tetrahedra will be depressed below the other two basal oxygens of each tetrahedron (Bailey 1984). The depressed oxygens form grooves or corrugations in the plane of basal oxygens (Bailey 1984).

When tetrahedral tilt and rotation are minimized the basal sheets can more easily coordinate with prismatic 6-fold coordination (Figure 15) around the K ion where the oxygen atoms in adjacent layers are superimposed over one another (the $n\cdot 60°$ rotation type). This type of interlayer cation bonding differs from 6-fold octahedral coordination (Figure 15) where the oxygen atoms are staggered in adjacent layers (the $n\cdot 120°$ rotation type). Lower Al content in the tetrahedral sheet reduces the amount of tetrahedral tilt and rotation needed for tetrahedral sheet and octahedral sheet articulation and also results in less basal oxygen corrugation. With less corrugation the basal oxygens are in a common plane, making $n\cdot 60°$ and $n\cdot 120°$ rotations more electrostatically equivalent. When tetrahedral Al substitution is high and octahedral Mg substitution is low, $n\cdot 120°$ rotations are the most favored because that is the best configuration to minimize basal oxygen repulsion.

Prismatic coordination does occur, although not as frequently, with Al-rich tetrahedra and octahedra in $2M_2$ muscovite. Muscovite with the $2M_2$ structure differs from the I/S described in this study in both composition and layer stacking. The $2M_2$ structure consists of regular alternations of layers by $\pm 60°$ and a consistent 1:4 Al to Si tetrahedral composition, whereas the I/S has a variable composition and a $1M$ stacking sequence with random rotations of $n\cdot 60°$. More work is needed to fully understand the structural relationships and physical conditions that result in the $2M_2$ structure. Another example of prismatic coordination is documented in glauconite by Sakharov *et al* (1990). An average glauconite composition is similar, although not identical, to the I/S samples from K-bentonites (Bailey

1980; Table 4). Like the I/S, glauconite has significant Mg and Fe octahedral substitution, but these two minerals formed in vastly different environments. It is not known what relative influences crystal-chemistry and environmental formation conditions play in determining the structural features and rotational stacking defects in I/S and other 2:1 layer phyllosilicates. In a hydrothermal alteration zone (Saskatchewan, Canada), Drits *et al* (1993) found illites with different octahedral cation distributions between *trans* and *cis* sites that had nearly identical chemical compositions. Their interpretation is that different physical conditions during the formation of the illite were responsible for the structural variations.

The observation that Al-rich I/S from K-bentonites is dominated by *cis*-vacant layers does not have a clear crystallographic explanation although some speculation may be worthwhile. Preliminary evidence indicates that the *cv-1M* structure is more stable than the *tv-1M* type (Drits *et al* 1993). In the *cv-1M* structure, the six K-O bond lengths are equal, whereas in the *tv-1M* structure K-O bond lengths are unequal, three being shorter and three being longer. In the case of a *trans*-occupied octahedra, the geometric center of the distorted hexagonal ring created by the basal oxygens of the top tetrahedral sheet is shifted $<a/3$ from the center of the corresponding ring on the bottom sheet (Tsipursky and Drits 1984, Drits *et al* 1993). In *trans*-vacant octahedra the geometric centers are shifted $>a/3$ from each other. In *trans*-vacant muscovite-$2M_1$ the interlayer K is not in the exact center of the distorted hexagonal ring but is displaced along the two-fold axis toward the vacant octahedral sites above and below resulting in unequal K-O bond lengths (Bailey 1984). Similar K-O bond length differences are likely for *trans*-vacant *1M* structures. There is less distortion of the tetrahedral sheets in the *cis*-vacant *1M* structure making a more regular interlayer cavity that results in nearly equal K-O bond lengths. Such differences in K bonding may affect the stability of these structures. However, it is still not clear at this time why Mg and Fe should favor the *tv* structure. The *cv* structure may be the most stable form of I/S for high Al and relatively low Mg compositions. However, more work is needed to verify this hypothesis. Geological considerations and associations concerning *cv* and *tv* I/S from K-bentonites will be given in a future paper.

CONCLUSIONS

The three-dimensional crystal structure of disordered I/S can be quantified by modeling random-powder X-ray diffraction patterns using the computer algorithm WILDFIRE (Reynolds 1993). Previously, diffraction patterns from rotationally disordered I/S that were strikingly different were described simply as *1Md*. The use of this modeling technique has enabled quantification of the amount and type of rotational disorder and the distribution of octahedral cations in the I/S examined here.

In the I/S from Ordovician and Devonian K-bentonites of the eastern United States, *cv* interstratification correlates with high tetrahedral Al, high octahedral Al and $n \cdot 120°$ rotational disorder. I/S that is dominated by *tv* octahedra correlate with low tetrahedral Al substitution, high octahedral Mg and Fe substitution and $n \cdot 60°$ rotational disorder. I/S expandability and Reichweite does not correlate systematically with *cv* interstratification and rotational disorder. The structural features in I/S result from some combination of their crystal chemistry and the environmental conditions under which the I/S formed.

ACKNOWLEDGMENTS

This research was supported in part by the American Chemical Society Grant 23613-AC2; Dartmouth College Earth Sciences Department, Hanover, NH; and the United States Geological Survey, Water Resources Division, Boulder, CO. Many of the samples in this study were generously donated by W. C. Elliott, W. D. Huff, R. L. Hay, and A. Chagnon who deserve special thanks. In addition, the writers are indebted to J. W. Delano, J. B. Droste, and S. P. Altaner for also supplying samples. The authors are indebted to Dr. Victor Drits for his review of this manuscript and elucidation concerning the structure of *cis*-vacant and *trans*-vacant unit-cells. We would also like to thank Dr. Dennis Eberl for help and support and the referees and editors for valuable comments.

REFERENCES

Altaner, S. P., and C. M. Bethke. 1988. Interlayer order in illite/smectite. *American Mineralogist* **73**: 766–774.

Bailey, S. W. 1966. The status of clay mineral structures. *Clays & Clay Miner.* **14**: 1–23.

Bailey, S. W. 1980. Structures of layer silicates. In *Crystal Structures of Clay Minerals and their X-Ray Identification.* G. W. Brindley and G. Brown, eds. London: Mineralogical Society, 1–124.

Bailey, S. W. 1984. Crystal chemistry of the true micas, Chapter 2. In *Micas.* S. W. Bailey, ed. Reviews in Mineralogy Vol. 13, Blacksburg, Virginia: Mineralogical Society of America, 13–60.

Bethke, C. M., and S. Marshak. 1990. Brine migrations across North American—The plate tectonics of groundwater. *Annu. Rev. Earth Planet Sci.* **18**: 287–315.

Dennison, J. M., and D. A. Textoris. 1970. Devonian Tioga tuff in northeastern United States. *Bulletin Volcanogenique* **34**: 289–293.

Dolasse, W. A. 1986. Correction of intensities for preferred orientation in powder diffractometry. Application of the March model. *J. Appl. Cryst.* **19**: 267–272.

Drits, V. A., B. A. Plançon, B. A. Sakharov, G. Besston, S. I. Tsipursky, and C. Tchoubar. 1984. Diffraction effects calculated for structural models of K-saturated montmorillonite containing different types of defects. *Clay Miner.* **19**: 541–561.

Drits, V. A., and C. Tchoubar. 1990. *X-ray Diffraction by Disordered Lamellar Structures.* New York: Springer-Verlag, 371 pp.

Drits, V. A., F. Weber, A. L. Salyn, and S. I. Tsipursky. 1993.

X-ray identification of one-layer illite varieties. Application to the study of illites around uranium deposits of Canada. *Clays & Clay Miner.* **41**: No. 3, 389–398.

Drits, V. A., and D. K. McCarty. 1995. The nature of diffraction effects from illite and illite/smectite consisting of interstratified *trans*-vacant and *cis*-vacant 2:1 layers; A semiquantitative technique for determination of layer-type content. *Amer. Miner.* (in review).

Droste, J. B., and C. J. Vitiliano. 1973. Tioga bentonite (Middle Ordovician) of Indiana. *Clays & Clay Miner.* **21**: 9–13.

Elliott, W. C., and J. L. Aronson. 1987. Alleghanian episode of K-bentonite illitization in the southern Appalachian basin. *Geology* **15**: 735–739.

Elliott, W. C., and J. L. Aronson. 1993. The timing and extent of illite formation in Ordovician K-bentonites at the Cincinnati Arch, Nashville Dome and north-eastern Illinois basin. *Basin Research* **5**: 125–135.

Güven, N. 1971. Structural factors controlling stacking sequences in dioctahedral micas. *Clays & Clay Miner.* **134**: 159–165.

Harris, A. G. 1979. Conodont color alteration, an organomineral metamorphic index and its application to Appalachian Basin geology. In *Aspects of Diagenesis.* P. A. Scholle and P. R. Schluger, eds. *Society of Economic Paleontologists and Mineralogists Special Publication* **26**: 3–16.

Hearn, P. P., J. F. Sutter, and H. E. Belkin. 1987. Evidence for Late-Paleozoic brine migration in Cambrian carbonate rocks of the central and southern Appalachians. Implications for Mississippi Valley-type sulfide mineralization. *Geochim. Cosmoch. Acta* **51**: 1323–1334.

Hower, J., E. V. Eslinger, M. E. Hower, and E. A. Perry. 1976. Mechanism of burial metamorphism of argillaceous sediment, mineralogical and chemical evidence. *Geol. Soc. of Amer. Bull.* **87**: 725–737.

Huff, W. D., and A. G. Türkmenoglu. 1981. Chemical characteristics and origin of Ordovician K-bentonites along the Cincinnati Arch. *Clays & Clay Miner.* **29**: 113–123.

Jennings, S., and G. R. Thompson. 1986. Digenesis of Plio-Pleistocene sediments of the Colorado River Delta, southern California. *J. Sed. Petrology* **56**: 89–98.

Johnsson, M. J. 1984. The thermal and burial history of south central New York: Evidence from vitrinite reflectance, clay mineral diagenesis and fission track dating of apatite and zircon: Masters thesis. Dartmouth College, Hanover, New Hampshire, 155 pp.

Kolata, D. R., J. K. Frost, and W. D. Huff. 1984. K-bentonites of the Ordovician Decorah Subgroup, upper Mississippi Valley: Correlation by chemical fingerprinting. *Illinois State Geological Survey, Circular 537,* 30 pp.

Maxwell, D. T., and J. Hower. 1967. High-grade diagenesis and low-grade metamorphism of illite in the Precambrian Belt Series. *Amer. Miner.* **52**: 843–857.

McCarty, D. K., and G. R. Thompson. 1991. Burial diagenesis in two Montana Tertiary basins. *Clays & Clay Miner.* **39**: 293–305.

Méring, J. and A. Oberlin. 1967. Electron-optical study of smectites: *Clays & Clay Miner.* 17th Nat. Conf., Pergamon Press, 3–25.

Mitchell, C. E. 1992. Chronostratigraphy of the Trenton Group and Utica Shale, Pt. I: Preliminary revision of lithofacies and age relationships. *Abstracts with Programs, 1992 GSA Annual Meeting,* Cincinnati, Ohio.

Moore, D. M., and R. C. Reynolds Jr. 1989. *X-ray Diffraction and the Identification and Analysis of Clay Minerals.* New York: Oxford University Press, 332 pp.

Oliver, J. 1986. Fluids expelled tectonically from orogenic belts: Their in hydrocarbon migration and other geologic phenomena. *Geology* **14**: 99–102.

Perry, E., and J. Hower. 1970. Burial diagenesis in Gulf Coast pelitic sediments. *Clays & Clay Miner.* **18**: 165–177.

Plançon, A. 1981. Diffraction by layer structures containing different kinds of layers and stacking faults. *J. Appl. Cryst.* **14**: 300–304.

Plançon, A., and C. Tchoubar. 1977a. Determination of structural defects in phyllosilicates by X-ray powder diffraction—I. Principle of calculation of the diffraction phenomenon. *Clays & Clay Miner.* **25**: 430–435.

Plançon, A., and C. Tchoubar. 1977b. Determination of structural defects in phyllosilicates by X-ray powder diffraction—II. Nature and proportion of defects in natural kaolinite. *Clays & Clay Miner.* **25**: 436–450.

Plançon, A., R. F. Giese, and R. Snyder. 1988. The Hinckley index for kaolinites. *Clay Miner.* **23**: 249–260.

Radoslovich, E. W. 1959. Structural control of polymorphism in micas. *Nature* **183**: 253–254.

Radoslovich, E. W., and K. Norrish. 1962. The cell dimensions and symmetry of layer lattice silicates. I. Some structural considerations. *Amer. Miner.* **47**: 599–616.

Reynolds, R. C. 1985. *NEWMOD computer program for the calculation of the one-dimensional X-ray diffraction patterns of mixed-layer clays.* R. C. Reynolds, ed. Dept. of Earth Sciences, Dartmouth College, Hanover, New Hampshire 03755.

Reynolds, R. C. 1992. X-ray diffraction studies of illite/smectite from rocks, <1 μm randomly oriented powders, and <1 μm oriented powder aggregates: The absence of laboratory-induced artifacts. *Clays & Clay Miner.* **40**: 387–396.

Reynolds, R. C. 1993. Three-dimensional powder X-ray diffraction from disordered illite: Simulation and interpretation of the diffraction patterns. In CMS Workshop Lectures, Vol. 5. *Computer Applications to X-ray Powder Diffraction Analysis of Clay Minerals.* R. C. Reynolds Jr. and J. R. Walker, eds. Boulder, Colorado: The Clay Minerals Society, 43–77.

Reynolds, R. C., and C. H. Thomson. 1993. Illite from the Potsdam Sandstone of New York: A probable noncentrosymmetric mica structure. *Clays & Clay Miner.* **41**: 66–72.

Roden, M. K., D. S. Miller, W. C. Elliott, and J. L. Aronson. 1992. The thermal history of the distal margin and interior of the southern Appalachian basin from combined fission-track and K/Ar studies of K-bentonites (abstract). *27th Annual Northeastern Section of the Geological Society of American Meeting* **24**, no. 3, p. 49.

Roden, M. K., W. C. Elliott, J. L. Aronson, and D. S. Miller. 1993. A comparison of fission-track ages of apatite and zircon to the K/Ar ages of illite/smectite (I/S) from Ordovician K-bentonites, southern Appalachian basin. *Journal of Geology* **101**: 633–641.

Sakharov, B. A., G. Besson, V. A. Drits, M. Yu Kamenava, A. L. Salyn, and B. B. Smoliar. 1990. X-ray study of the nature of stacking faults in the structure of glauconites. *Clay Miner.* **25**: 419–435.

Środoń, J., D. J. Morgan, E. V. Eslinger, D. D. Eberl, and M. R. Karlinger. 1986. Chemistry of illite/smectite and end-member illite. *Clays & Clay Miner.* **34**: 368–378.

Tsipursky, S. I., and V. A. Drits. 1984. The distribution of octahedral cations in the 2:1 layers of dioctahedral smectites studied by oblique-texture electron diffraction. *Clay Miner.* **19**: 177–193.

Velde, B. 1965. Experimental determination of muscovite polymorph stabilities. *Amer. Miner.* **50**: 436–449.

Yoder, H. S., and H. P. Eugster. 1955. Synthetic and natural muscovites. *Geochim. Cosmochim. Acta* **8**: 225–280.

(Received 8 February 1994; accepted 29 September 1994; Ms. 2467)